

# **Biocatalytically active and stable cross-linked enzyme crystals of halohydrin dehalogenase HheG by protein engineering**

Marcel Staar,<sup>[a]</sup> Steffi Henke,<sup>[b]</sup> Wulf Blankenfeldt,<sup>[b]</sup> Anett Schallmeyer\*<sup>[a]</sup>

[a] Marcel Staar, Anett Schallmeyer

Institute for Biochemistry, Biotechnology and Bioinformatics, Technical University Braunschweig,  
Spielmannstr. 7, 38106 Braunschweig, Germany

[b] Steffi Henke, Wulf Blankenfeldt

Structure and Function of Proteins, Helmholtz Centre for Infection Research, Inhoffenstr. 7, 38124  
Braunschweig, Germany

## **\* Correspondance**

Anett Schallmeyer, Institute for Biochemistry, Biotechnology and Bioinformatics, Technical University  
Braunschweig, Spielmannstr. 7, 38106 Braunschweig, Germany.

Email: a.schallmeyer@tu-braunschweig.de

## **Abstract**

A major drawback for practical application of halohydrin dehalogenase HheG in biocatalysis is its rather low thermal stability and low organic solvent tolerance. We therefore pursued a stabilization of HheG via immobilization as cross-linked enzyme crystals. Since glutaraldehyde inactivates HheG, we introduced a cysteine residue in the crystal interface, which enabled thiol-specific cross-linking at predefined cross-linking sites. Variant HheG D114C displayed improved crystallizability and yielded stable and catalytically active CLECs using bis-maleimidoethane as cross-linker. Effective cross-linking at the predefined site could be confirmed via the CLEC crystal structure. Compared to soluble enzyme, the CLECs displayed significantly improved stability and activity at higher temperatures, lower pH values and in the presence of water-miscible organic solvents, which enabled their reuse over 21 days in the azidolysis of cyclohexene oxide.

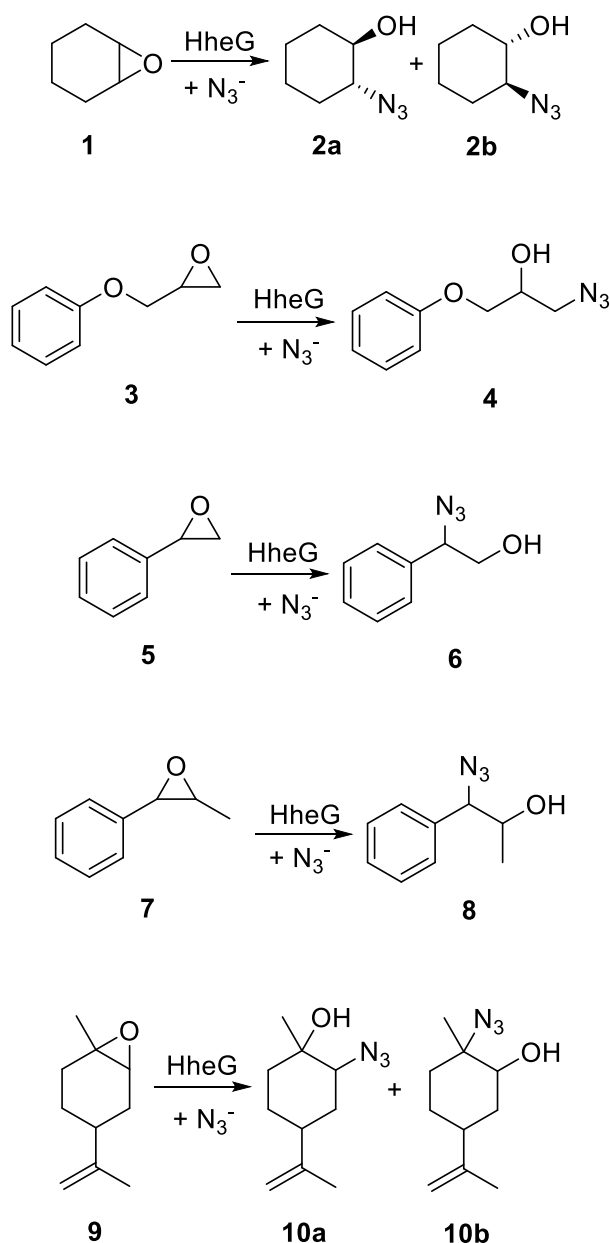
## **Introduction**

Halohydrin dehalogenases (HHDHs) (E.C. 4.5.1.-) are bacterial lyases belonging to the superfamily of short-chain dehydrogenases/reductases. While their natural function is the dehalogenation of vicinal haloalcohols with concomitant epoxide formation,<sup>[1]</sup> they are also able to catalyze the reverse reaction, i.e. epoxide-ring opening, with a range of different nucleophiles enabling formation of C-C, C-N, C-O and C-S bonds.<sup>[2]</sup> This has made HHDHs attractive for application in biocatalysis and various examples, e.g. for the synthesis of enantioenriched oxazolidinones, tertiary alcohols, epihalohydrines or spiroepoxyoxindoles, using HHDH-catalysis have been reported in literature.<sup>[3–6]</sup>

Using a database mining approach based on HHDH-specific sequence motifs,<sup>[7]</sup> a large number of new halohydrin dehalogenases have been identified in public sequence databases in recent years<sup>[1]</sup> and several new members have been characterized as well.<sup>[8]</sup> While most HHDHs display similar substrate scopes, HheG from *Ilumatobacter coccineus* also accepts sterically more demanding cyclic epoxides as well as acyclic non-terminal epoxide substrates.<sup>[9,10]</sup> Additionally, HheG displays  $\alpha$ -regioselectivity in the ring-opening of different styrene oxide derivatives,<sup>[11]</sup> whereas other HHDHs exclusively attack the  $\beta$ -carbon of the epoxide ring. Solving the crystal structure of HheG<sup>[9]</sup> revealed a much broader active site for this enzyme compared to other HHDHs,<sup>[12–15]</sup> which explains the acceptance of bulkier substrates. This feature makes HheG very attractive for industrial application, e.g. for the synthesis of pharmaceutical building blocks.<sup>[16]</sup> A major drawback for application, however, is the enzyme's low stability (apparent melting temperature  $T_m$  of only 38 °C) and its low organic solvent tolerance.<sup>[17]</sup> Based on protein engineering of HheG, variants with amino acid exchanges at position T123 have been obtained displaying up to 14 K higher  $T_m$  as well as up to three-fold higher activity, resulting also in a slight increase in organic solvent resistance.<sup>[17]</sup>

To complement our protein engineering efforts with HheG, we herein report an orthogonal strategy to the stabilization of HheG using immobilization.<sup>[18]</sup> Common enzyme immobilization methods include carrier binding, polymer entrapment, and carrier-free immobilization methods based on cross-linking such as cross-linked enzyme crystals (CLECs) or cross-linked enzyme aggregates (CLEAs).<sup>[19]</sup> Since wild-type HheG crystallizes readily after a single IMAC purification step, we opted for CLEC generation to obtain an immobilized HheG preparation that would still be active at higher cosolvent concentration, and that could be reused. CLECs of various enzymes have previously been reported to display high stability regarding temperature and pH, also in extreme conditions, and have been applied for biocatalytic reactions in non-conventional reaction media.<sup>[20–22]</sup> The most common cross-linker used for CLEC formation is glutaraldehyde, which reacts primarily with  $\epsilon$ -amino groups of lysines, but is also able to cross-link arginine and tyrosine side chains.<sup>[23]</sup> Previous attempts, however, to cross-link HheG crystals with glutaraldehyde via soaking resulted only in inactive CLECs. The high excess of glutaraldehyde during cross-linking likely also resulted in cross-linking of Tyr165 and Arg169 of the

catalytic triad of HheG. In contrast, cross-linking of HheG crystals with glutaraldehyde via vapor diffusion yielded CLECs that still displayed activity in the ring opening of cyclohexene oxide (**1**) with azide (Scheme 1).<sup>[24]</sup> This approach, however, is impractical in larger scales where protein crystallization is generally performed in stirred vessels.<sup>[25]</sup> Hence, we herein attempted to use protein engineering of HheG to insert desired residues in crystal contacts that would allow us to use chemoselective cross-linkers for stable CLEC generation without compromising biocatalyst activity.



**Scheme 1.** Epoxide ring opening reactions of HheG performed in this study [**1**: cyclohexene oxide, **2a**: (1*R*,2*R*)-2-azido-1-cyclohexanol, **2b**: (1*S*,2*S*)-2-azido-1-cyclohexanol, **3**: glycidylphenylether, **4**: 1-azido-3-phenoxy-propan-2-ol; **5**: styrene oxide, **6**: 2-azido-2-phenylethanol, **7**: *trans*-1-phenylpropylene oxide, **8**: 1-azido-1-phenylpropan-2-ol, **9**: (+)-*cis/trans*-limonene oxide, **10a**: 2-azido-1-methyl-4-(prop-1-en-2-yl)cyclohexan-1-ol, **10b**: 2-azido-2-methyl-5-(prop-1-en-2-yl)cyclohexan-1-ol.

## **Results and Discussion**

### ***Crystal contact engineering***

As the previous cross-linking of HheG crystals with the commonly used cross-linker glutaraldehyde significantly reduced enzyme activity, protein engineering of HheG was used herein to introduce desired amino acids on the enzyme surface as new cross-linking sites for alternative cross-linkers. Specifically, we aimed for the insertion of cysteine residues, as HheG wild type contains only few cysteines that could potentially be cross-linked as well. Thus, the available crystal structure of wild-type HheG<sup>[9]</sup> was analyzed for potential residues facing each other in the crystal interface. As shown in Figure 1, two major interfaces (contact points) between HheG tetramers within the crystal can be distinguished: an axial and a tangential interface. The axial interface refers to crystal contacts between tetramers lining up in infinite strings throughout the crystal, while the tangential interface represents crystal contacts between tetramers of orthogonal strings. Existing crystal contacts were analyzed using the PRODIGY crystal webserver<sup>[26]</sup> to identify residues with less than 5 Å distance to each other. Interestingly, this revealed three residues with the same amino acid positions of different HheG tetramers facing each other in the crystal interfaces: M45 and D114 in the axial interface, and A221 in the tangential interface (Figure 1B). Those residues were selected for replacement by cysteine, as mutagenesis of one residue would directly result in the required cysteine pairs of neighbouring tetramers for later cross-linking. As the C<sub>α</sub> distances of those opposing residues are between 6.5-8.5 Å (Table S1), bis-maleimidoethane (BMOE) with a spacer length of 8 Å was selected as thiol-specific cross-linker for later CLEC generation (Figure S1).<sup>[27]</sup>

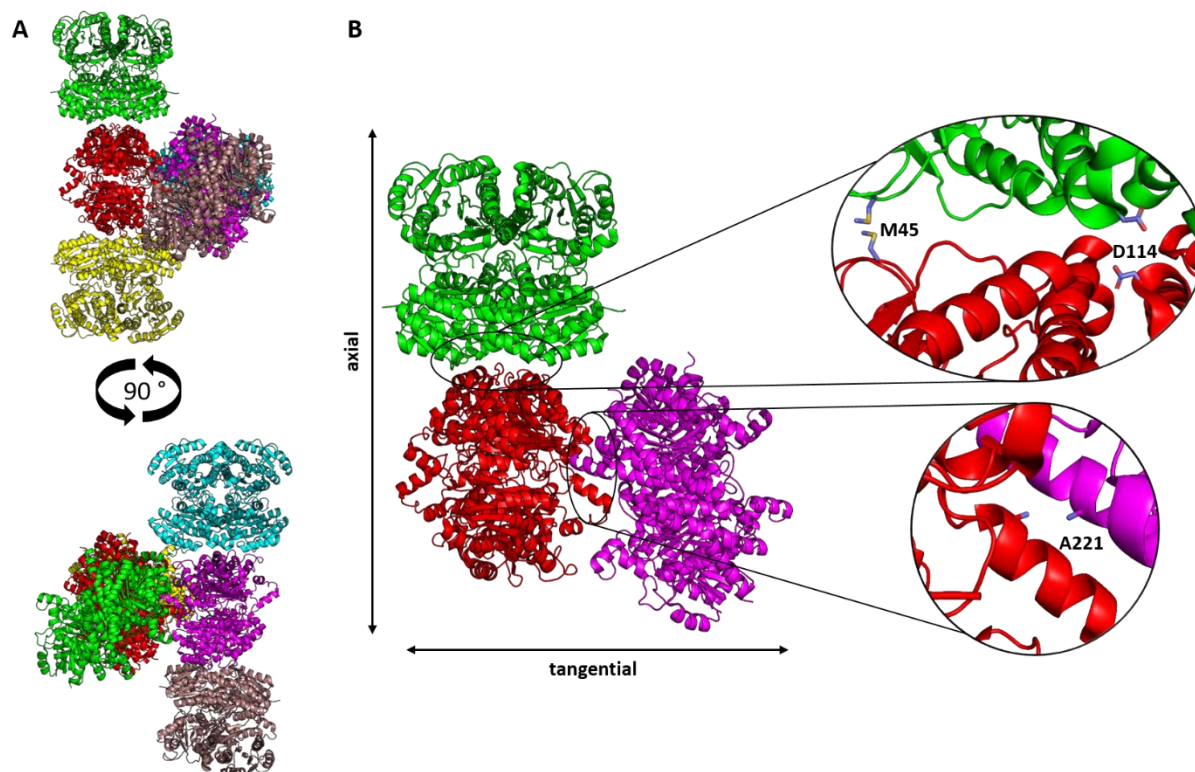


**Figure 1.** Crystal contact analysis of wild-type HheG (PDB ID: 5O30). **A)** Arrangement of HheG tetramers within the unit cell; **B)** Axial and tangential crystal contacts of HheG with positions M45, D114 and A221 highlighted.

HheG variants M45C, D114C and A221C were generated, produced in *E. coli* and purified according to established protocols for wild-type HheG. Corresponding yields after purification are listed in Table 1. Before crystallization and cross-linking, these mutants were characterized regarding their specific activity, enantioselectivity and thermal stability for comparison with the wild-type enzyme (Table 1).

**Table 1.** Specific activities and product enantiomeric excess ( $ee_p$ ) in the conversion of cyclohexene oxide (**1**) with azide as nucleophile, as well as melting temperatures ( $T_m$ ) of HheG wild type and respective variants applied as soluble enzymes. Specific activity and product enantiomeric excess ( $ee_p$ ) were determined based on duplicate measurements, apparent melting temperatures ( $T_m$ ) where obtained from triplicate measurements.

Variant	Yield [mg/l]	Specific activity <sup>a</sup> [U/mg]	$ee_p$ [%]	$T_m$ [°C]
WT	204	$2.32 \pm 0.3$	$49.1 \pm 0.1$	$41 \pm 0.1$
M45C	22	$1.41 \pm 0.01$	$65.4 \pm 0.1$	$42.5 \pm 0.2$
D114C	130	$2.35 \pm 0.05$	$49.9 \pm 0.5$	$40.5 \pm 0.2$
A221C	190	$1.79 \pm 0.1$	$49.5 \pm 0.8$	$40 \pm 0.1$

<sup>a</sup> Reaction conditions: 20 mM cyclohexene oxide (**1**), 40 mM azide and 50  $\mu$ g enzyme in 1.5 ml 50 mM Tris $\cdot$ SO<sub>4</sub>, pH 7.0 at 22 °C and 900 rpm

This analysis revealed a similar activity and enantioselectivity of HheG D114C for formation of azidoalcohol **2b** and a similar melting temperature ( $T_m$ ) as determined for HheG wild type. In contrast, variant M45C displayed significantly reduced specific activity, while product **2b** was obtained with higher enantiomeric excess. As replacement of M45 by cysteine significantly altered the biochemical characteristics of this variant compared to wild-type HheG, this variant was not investigated further. The specific activity of HheG A221C was also reduced (75% of wild-type activity), whereas product enantiomeric excess and  $T_m$  were similar to that of HheG wild type. Since HheG A221C was the only variant with a cysteine pair for cross-linking in the tangential crystal interface, this variant was included in further studies, despite its slightly reduced specific activity. Both variants, D114C and A221C, as well as wild-type HheG, were further compared regarding their crystallization properties.

### ***Crystallization and cross-linking***

Crystallization of HheG wild type had previously been demonstrated using 10% (w/v) PEG4000 as precipitant, HEPES buffer with a pH of 7.3 to 7.5 and protein concentrations between 6 and 32 mg/ml.<sup>[24,28]</sup> Hence, similar conditions were used to investigate the crystallizability of variants D114C and A221C (see supplementary for more details). This revealed that variant D114C displayed a higher crystallizability and required less PEG4000 compared to HheG wild type, while no crystals could be obtained for variant A221C (Table S2). Moreover, variant D114C still gave the same hexagonal-shaped crystals as wild-type HheG (Figure S2), but crystallized faster (Figure S3) and formed overall larger crystals (Figure S4). As the space group and cell parameters of D114C crystals were found to be the same or very similar to that of wild-type HheG (see below), the mutation at position 114 is likely responsible for improved crystallizability of variant D114C. In wild-type HheG, always two D114 residues of opposing tetramers face each other in the axial crystal interface, most likely resulting in a slight repulsion of the charged carboxyl side chains during crystallization. In contrast, the thiols in variant D114C (cysteine  $pK_a = 8.1$ ) are only partially charged at the pH used for crystallization. Moreover, mutation D114C might result in a lower conformational entropy of the amino acid side chains at position 114, which would also contribute to improved protein crystallization.<sup>[29,30]</sup>

After crystallization of HheG wild type and D114C at 20  $\mu$ l scale, cross-linking of both variants with the cysteine-specific cross-linker BMOE was tested. As expected, crystals of HheG wild type incubated with 2 mM BMOE for 24 h re-dissolved within 72 h after transfer into reaction buffer (Figure S5). In contrast, respective crystals of HheG D114C did not re-dissolve after cross-linking with 2 mM BMOE for 24 h

(Figure S6). This indicates that only HheG D114C crystals offer suitable cross-linking sites for stable cross-linking with BMOE.

For the stable CLECs, the activity in the conversion of cyclohexene oxide (**1**) with azide was subsequently examined and compared to soluble enzyme preparations (Figure 2). As mentioned previously, CLECs of HheG wild type cross-linked with glutaraldehyde via soaking displayed only negligible residual activity in the range of the chemical background. In contrast, HheG D114C CLECs cross-linked with BMOE via soaking displayed high conversion in the azidolysis of **1**, albeit at 4 h reaction time conversion is slightly lower compared to the soluble enzyme (Figure 2). The latter, however, might be due to diffusion limitations within the crystal,<sup>[24,31]</sup> reducing substrate accessibility and product release. On the other hand, the limited enzyme motion within the CLEC could also explain the observed activity decrease.

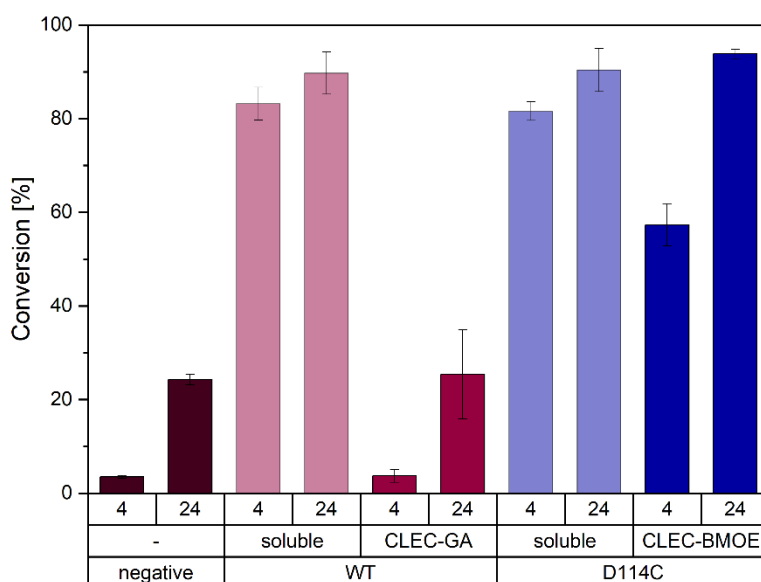


**Figure 2.** Conversion of 20 mM cyclohexene oxide (**1**) with 40 mM azide using HheG WT and mutant D114C (each 100  $\mu$ g) in soluble or CLEC form after 4 and 24 h of reaction [GA: glutaraldehyde]. “Negative” represents the chemical background reaction without enzyme addition. Error bars indicate standard deviations from five parallel reactions.

Literature reports indicated that cross-linking can also have a positive effect on the enantioselectivity of an enzyme.<sup>[32]</sup> Thus, the enantioselectivity of our CLECs in the conversion of **1** was investigated as well. Interestingly, HheG D114C CLECs formed azidoalcohol **2** with slightly higher product enantiomeric excess than the respective soluble enzyme (56.0% vs 49.9%, respectively). This might be explained by reduced molecular motion of enzyme molecules within the crystal due to cross-linking.<sup>[33]</sup>

Moreover, an 8 K increase in apparent melting temperature ( $T_m$ ) compared to soluble enzyme was observed for D114C CLECs cross-linked with BMOE (Figure S7). This gain in melting temperature was

also obtained when using only 0.5 mM BMOE and a cross-linking time of 24 h, as well as with 2 mM BMOE and 3 h cross-linking time (Figure S8). This demonstrates the effectiveness of BMOE as cross-linker for HheG D114C crystals. Using higher cross-linker concentrations or longer cross-linking times did not enhance CLEC stability further (Figure S8). For comparison, cross-linking of wild-type HheG crystals with glutaraldehyde yielded a  $T_m$  increase by 9 K (data not shown).

### ***Crystal structure of HheG D114C CLEC***

To confirm effective cross-linking of HheG D114C crystals with BMOE, the crystal structure of respective CLECs was solved at 2.7 Å resolution (PDB-ID: 7QY3). Variant D114C crystallized in the same trigonal space group  $P3_121$  as wild-type HheG.<sup>[9]</sup> Moreover, unit cell parameters were also similar to that of the wild-type enzyme (Table S3). Analysis via PDBePISA webserver<sup>[34]</sup> confirmed that crystals of variant D114C exhibited the same crystal contacts (axial and tangential interface, see Figure 1) as wild-type HheG except for the mutated residue 114, where an aspartic acid was exchanged by a cysteine. In an overlay of both structures (Figure 3A), residue 114 – either aspartic acid in wild-type HheG or cysteine in variant D114C – adopts the same position and conformation.

As can be seen in Figure 3C, additional electron density between cysteines at position 114, facing each other in the crystal contact, is present in the HheG D114C structure. The shape and size of this additional electron density fit to that of the cross-linker BMOE, confirming effective cross-linking at the desired position. This extra density can be found for every cysteine 114 within the asymmetric unit, suggesting a high degree of cross-linking with BMOE for HheG D114C CLECs. Interestingly, there is no previous literature precedent, where cross-links within a biocatalytic CLEC could be visualized. This is explained by the fact that previously glutaraldehyde has been used almost exclusively as cross-linker for CLEC generation.<sup>[35]</sup> As mentioned before, glutaraldehyde is able to react with different amino acids within a protein and is further prone to polymerization. This results in a multitude of cross-linking possibilities that will be occupied only randomly within a CLEC, hampering visualization by X-ray crystallography.<sup>[36,37]</sup> In contrast, our approach yields highly defined cross-linking sites for stable CLEC generation and, thus, permits also visualization of resulting cross-links.

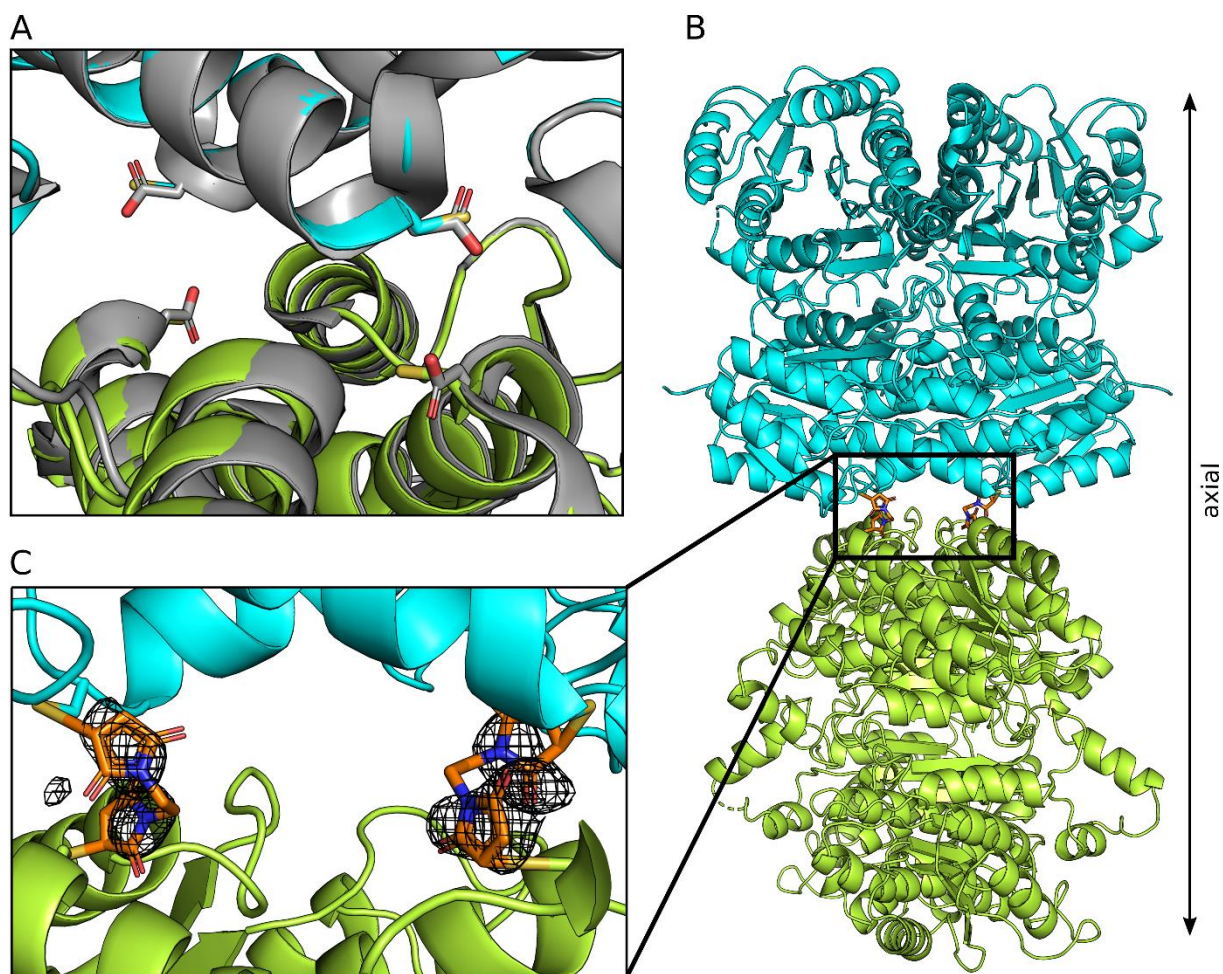


**Figure 3.** Crystal structure of HheG D114C. **A)** Overlay of residue 114 of variant HheG D114C (colored) and the wild-type structure (gray). **B)** Cross-linked chains of neighboring tetramers in axial orientation, BMOE shown in orange. **C)** Magnified view of the bound cross-linker BMOE fitting into the respective electron density ( $(F_o - F_c)$  at  $3\sigma$ ).

#### **Further CLEC characterization**

As a higher melting temperature has been observed for HheG D114C CLECs cross-linked with BMOE, we further investigated the temperature and pH profile of such CLECs. In line with the observed higher  $T_m$ , HheG D114C CLECs displayed their highest relative activity at 40°C in the azidolysis of **1**, while highest relative activity of soluble enzyme was obtained at 25°C (Figure 4A). Moreover, also the determined  $T_{50}$  value of HheG D114C CLECs was 12 K higher compared to soluble enzyme (Figure S9), further confirming an increased thermal stability upon CLEC formation.

Interestingly, the pH profile of the CLECs broadened compared to soluble enzyme, specifically with respect to performance at lower pH values, while the pH optimum stayed at pH=6 (Figure 4B). This pH optimum is in line with the catalytic mechanism of HDDHs for epoxide ring opening, with Tyr165 of the catalytic triad donating a proton to the oxyanion generated during epoxide ring opening.<sup>[9]</sup> While acidic

pH will facilitate reprotonation of Tyr165 for the next catalytic cycle, the enzyme is inactivated at low pH values (Figure 4B). The latter is accompanied by a reduced enzyme stability at acidic pH, which was partially mitigated by cross-linking. In line with these results, CLECs exhibited also significantly higher  $T_m$  values at lower pH compared to soluble enzyme (Figure S10).

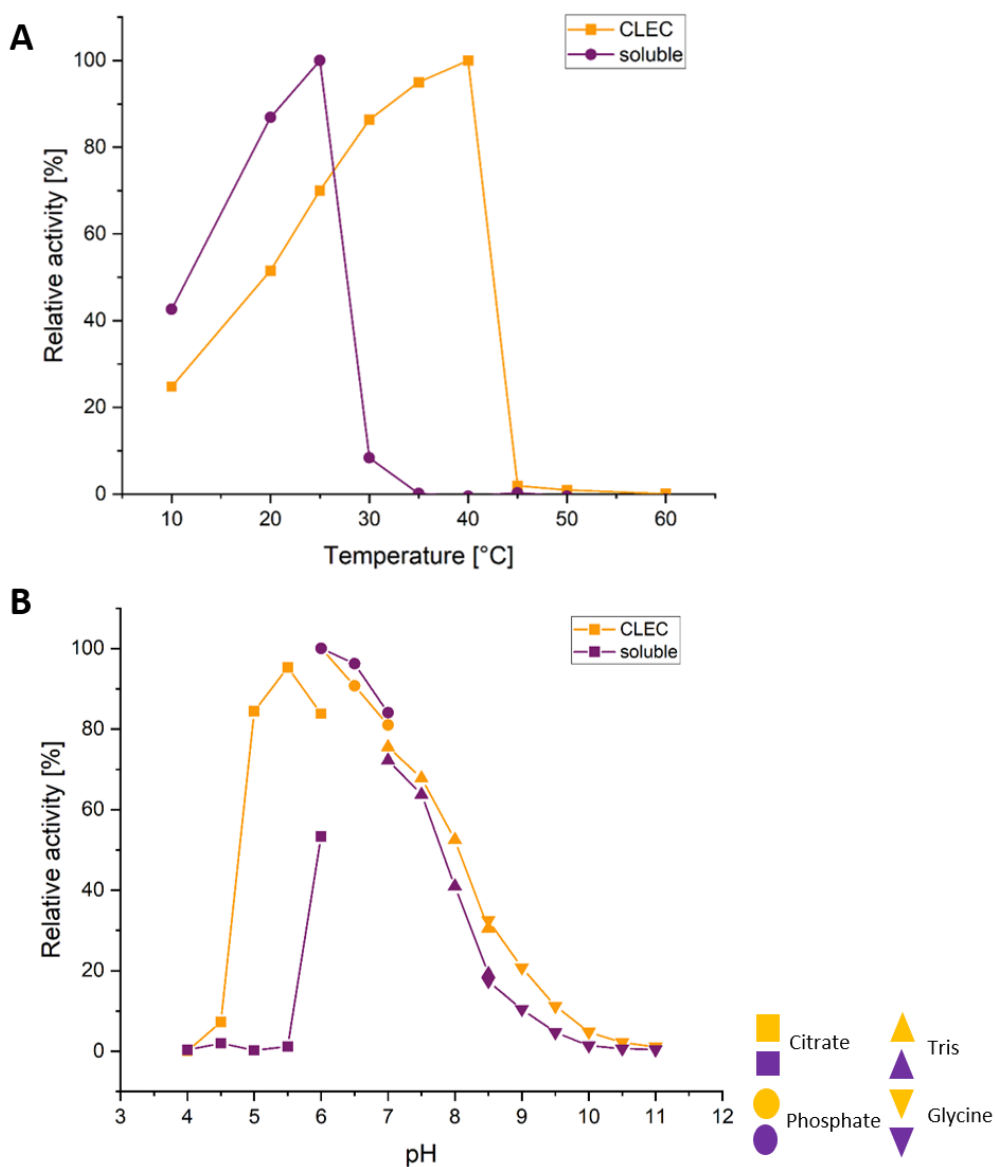


**Figure 4.** Temperature (A) and pH (B) profiles of HheG D114C CLECs (black) in comparison to soluble enzyme (red) in the conversion of 20 mM cyclohexene oxide (1) with 40 mM azide at 22°C using each 100 µg of enzyme. Relative activities have been calculated by setting the highest conversion to 100% activity. For temperature profile 100% relative activity corresponds to 64.1% (soluble) or 48.3% (CLEC) conversion. For pH profile 100% relative activity corresponds to 85.5% (soluble) or 71.4% (CLEC) conversion.

Previous literature on cross-linked enzyme crystals of *Candida rugosa* lipase and *Pseudomonas cepacia* lipase, as well as CLECs of the protease subtilisin reported improved activity and stability of respective CLECs in organic solvents compared to soluble enzymes.<sup>[20,21]</sup> Organic co-solvents are usually required to increase substrate solubility in HHDH-catalyzed reactions. Previously, however, significantly reduced activity/stability of HheG in the presence of different water-miscible organic solvents has been observed.<sup>[17]</sup> Hence, we also investigated the activity of HheG D114C CLECs in the presence of 25% (v/v) of various co-solvents. In comparison to soluble enzyme, D114C CLECs were still active in the presence of 25% (v/v) DMF, methanol, ethanol and isopropanol, whereas soluble enzyme seemed to be fully inactivated at this solvent concentration (Figure 5). In contrast, the achieved conversion of soluble HheG D114C in the presence of 25% (v/v) DMSO for the azidolysis of **1** was similar to the respective conversion obtained with the CLECs, while for both enzyme preparations no activity could be observed with 25% (v/v) acetonitrile. Moreover, melting temperatures of HheG D114C CLECs and soluble enzyme in the presence of 10% (v/v) co-solvents have been determined (Table S4), which clearly indicate that acetonitrile has the highest destabilizing effect on both enzyme preparations. In contrast, the influence of DMSO on D114C stability (soluble and CLEC form) seems only marginal. Both results are in line with obtained conversion data (Figure 5). According to  $T_m$  measurements, D114C CLECs are more stable in the presence of 10% (v/v) organic co-solvent compared to soluble enzyme for all co-solvents tested (Table S4), again confirming their higher overall stability.

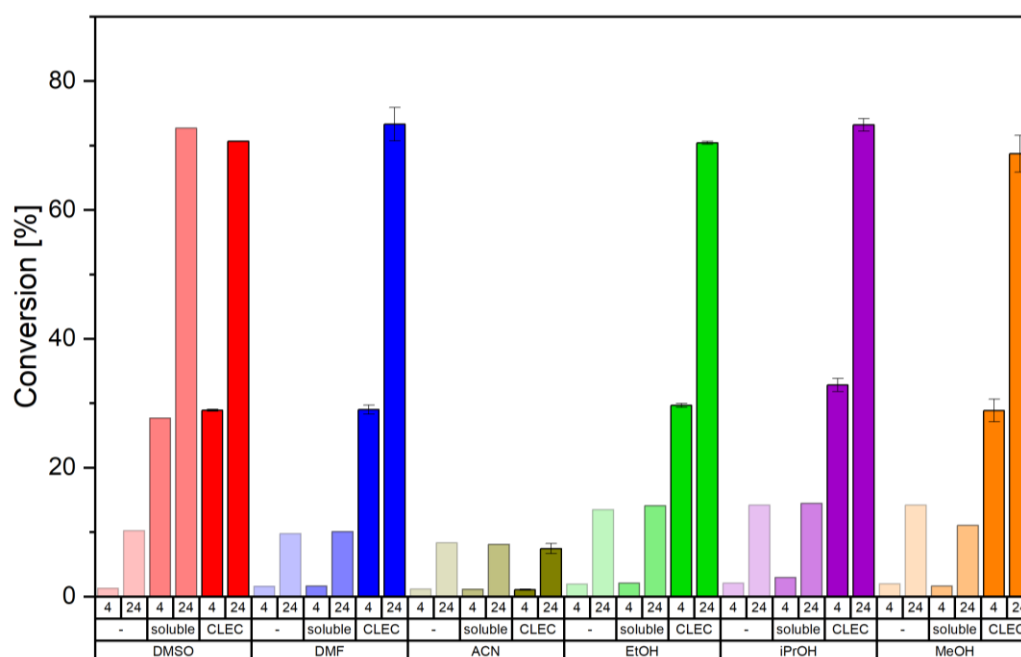


**Figure 5.** Influence of 25% (v/v) co-solvent on HheG D114C CLECs and soluble enzyme in the conversion of 20 mM cyclohexene oxide (**1**) with 40 mM azide at 22°C using each 100 µg enzyme. Used co-solvents: dimethyl sulfoxide (DMSO), dimethyl formamide (DMF), acetonitrile (ACN), ethanol (EtOH),

isopropanol (iPrOH) and methanol (MeOH). Samples were taken after 4 and 24 h. “-” indicates negative control reactions without enzyme addition. All reactions were performed in duplicate.

The observed higher stability of D114C CLECs in the presence of organic co-solvents enabled also the use of significantly higher substrate concentrations in the azidolysis of **1**. Specifically, D114C CLECs were still active at the highest substrate concentration tested (200 mM **1** at 20% (v/v) isopropanol), while soluble enzyme was fully inactive already (Figure S11). This result further confirms the significantly increased stability of D114C CLECs in the presence of water-miscible organic solvents.

To evaluate also long-term stability of our CLECs at the used reaction temperature (22 °C), half-life times ( $t_{1/2}$ ) of soluble enzyme and CLECs of HheG D114C were investigated. To facilitate the determination of  $t_{1/2}$  at 22°C, deactivation rate constants  $k_d$  of soluble enzyme and CLECs at higher temperatures (>30°C) were determined. Using the Eyring equation<sup>[38]</sup>, respective deactivation rate constants at 22°C could be extrapolated (Figure S12), and deactivation energies as well as half-life times were determined (Table S6). As a result, a half-life time of 64 days at 22°C was obtained for D114C CLECs, which is consistent with our reusability data (see below). In contrast, the respective  $t_{1/2}$  of soluble enzyme at 22°C is only 21 h. Hence, D114C CLECs exhibit a more than 60 times higher half life than soluble HheG D114C. Similar increases in half life upon CLEC formation have also been reported for other enzymes.<sup>[39,40]</sup> Likewise, more energy is required for the deactivation of HheG D114C CLECs (46.8 kJ/mol) in comparison to soluble enzyme (36.3 kJ/mol), underlining once more the significant gain in stability upon cross-linking.

### **Application of HheG D114C CLECs in biocatalytic reactions**

Apart from higher stability, immobilization of an enzyme as CLEC also offers the advantage of easy enzyme recovery from a product stream<sup>[35]</sup> and reuse in biocatalytic reactions. Therefore, repeated batch reactions with cyclohexene oxide (**1**) and azide at 22°C were performed for each 24 h with daily reuse of D114C CLECs over a total of 21 days. After each reaction, the CLECs were separated by centrifugation before reuse in a new batch reaction. As shown in Figure 6, D114C CLECs displayed activity over all reaction cycles, obtaining still 87% and 70% of the initially observed conversion after 5 and 21 days, respectively. The observed slight decrease in enantiomeric excess during this time span can be explained by a stronger influence of the chemical background reaction with decreasing enzyme activity. Microscopic analysis of the D114C CLECs after the 21 reaction cycles confirmed that they retained their hexagonal shape with sizes of about 100  $\mu\text{m}$  (Figure S13).

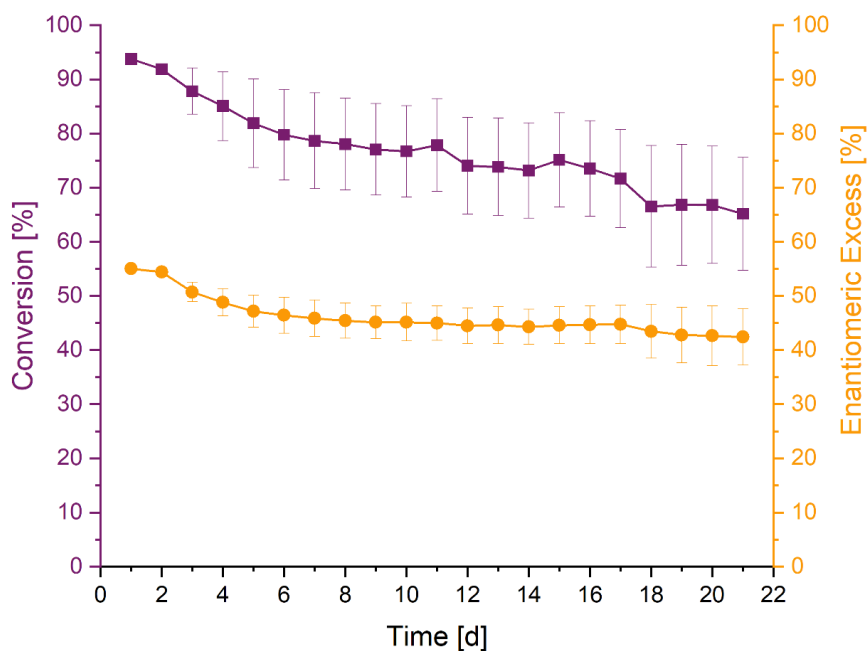


**Figure 6.** Repetitive batch reactions with cyclohexene oxide (**1**) and azide at 22°C with reuse of HheG D114C CLECs. Each reaction cycle (24 h) contained 100 µg CLECs, 20 mM cyclohexene oxide (**1**) and 40 mM azide in a total of 1 mL. After 24 h of reaction, the CLECs were centrifuged, the supernatant was removed and fresh reaction media including the substrates was added to start a new cycle. Standard deviations are based on quintuple measurements. For comparison, chemical background conversion in this reaction (one cycle) without enzyme addition reached 24%.

In addition to cyclohexene oxide, we also tested the application and reuse of D114C CLECs in the azidolysis of phenylglycidylether (**3**)<sup>[8]</sup>, styrene oxide (**5**)<sup>[11]</sup>, phenylpropylene oxide (**7**)<sup>[10]</sup> and limonene oxide (**9**)<sup>[9]</sup>, which had been demonstrated previously to be converted by HheG. Daily reuse of D114C CLECs over 5 cycles yielded no or only a slight decrease in conversion with these four epoxide substrates (Figure S14). The activity recovery comparing conversion in the first and fifth cycle was 99.4% (**3**), 100% (**5**), 93.9% (**7**) and 91.1% (**9**). In comparison, CLEAs of HheC from *Agrobacterium radiobacter* AD1 displayed an activity recovery of 74% after 10 reaction cycles of each 30 min in the conversion of 5 mM 1,3-dichloro-2-propanol.<sup>[41]</sup> Hence, our data demonstrate the effectiveness of HheG immobilization via CLEC formation to obtain a stable and reusable biocatalyst.

Additionally, storage stability of D114C CLECs at 8°C was investigated yielding 98.7% residual activity after 1 week and 83.3% after 1 month of storage.

## **Conclusion**

In conclusion, we employed crystal contact engineering to generate CLECs of HheG with chemo-selective cross-linking at predefined cross-linking sites. To this end, HheG variant D114C was generated

for stable cross-linking with the thiol-specific cross-linker BMOE. In contrast to CLECs generated with the commonly used cross-linker glutaraldehyde, this approach yielded selective cross-linking at well-defined sites without compromising enzyme activity. The resulting CLECs not only displayed significantly higher stability regarding temperature, pH and co-solvent concentrations compared to the soluble enzyme, but also enabled the repetitive use of HheG in the azidolysis of various epoxide substrates (up to 21 days as shown for the conversion of cyclohexene oxide). Overall, those CLECs represent an important first step towards a potential future application of HheG in industrial settings. Furthermore, the cross-linking approach described herein can be easily transferred to other biocatalysts with high crystallizability that would typically be inactivated upon cross-linking with glutaraldehyde. Building on the variety of commercially available mono- and bi-specific crosslinkers, this approach should further allow crosslinking beyond the thiol functionality. Even the use of cleavable cross-linkers is conceivable, opening up a whole range of new possibilities for future applications.

## **Experimental Section**

### ***Chemicals***

Substrates cyclohexene oxide (**1**) and styrene oxide (**5**) were purchased from Thermo Fisher Scientific (Geel, Belgium). Substrates phenylglycidylether (**3**), phenylpropylene oxide (**7**) and limonene oxide (**9**) were purchased from Merck (Darmstadt, Germany). All chemicals were of highest available purity.

### ***Bacterial strains and plasmids***

*E. coli* DH5 $\alpha$  was used for cloning and other genetic manipulations whereas *E. coli* BL21(DE3) Gold was used for heterologous protein production as outlined before.<sup>[8]</sup> Further, expression vector pET-28a(+) (Merck) was used to clone respective genes under control of the T7 promoter while adding an N-terminal His<sub>6</sub>-tag to heterologously produced proteins.

### ***HheG engineering***

Amino acid positions were selected based on their position at the crystal interface. Symmetry mates of HheG were generated using PyMOL (version 2.3.3, Schrödinger, New York, NY, United States). This way, amino acids facing each other within a distance of less than 5 Å at the crystal interface were selected by the PRODIGY crystal webserver.<sup>[26]</sup> Site-directed mutagenesis was performed using the PfuUltra II Hotstart PCR Mastermix (Agilent Technologies, Santa-Clara, CA, United States). Forward and reverse mutagenic primers (Table 2) were designed with PrimerX (Carlo Lapid, 2003, <http://bioinformatics.org/primerx/index.htm>), purchased from Merck and used in concentrations of 0.25  $\mu$ M each with 100 ng of pET28a(+)-*hheG* template.<sup>[17]</sup> Otherwise, the mutagenesis protocol was in agreement with the manufacturer's instructions.

**Table 2.** Mutagenic primers used in this study. Base exchanges are shown in bold.

<b>Mutagenic primer</b>	<b>Sequence 5'-3'</b>
f_hheG_M45C	CAGCCGGTGATGGCACCT <b>GCG</b> TTGGTGTGAAGAAAG
r_hheG_M45C	CTTTCTCAACACCAAC <b>GCA</b> GGTGCCATCACCGGCTG
f_hheG_D114C	CGGCAAATTTCTGGATATGACCT <b>GCG</b> GATCAGTGGGCAAAAGTTAAAG
r_hheG_D114C	CTTAACTTTTGCCCACTGAT <b>GCA</b> GGTCATATCCAGAAATTTGCCG
f_hheG_A221C	CGTCGTGCAATGATTGAAT <b>GCC</b> AGGTTCCGCTGCGTCCG
r_hheG_A221C	CGACGCAGCGGAACCT <b>GCA</b> TTCAATCATTGCACGACG

### ***Protein production and purification***

HheG and its variants were produced in 500 ml Terrific Broth (TB) (per liter: 4 ml glycerol, 12 g peptone, 24 g yeast extract, 0.17 M  $\text{KH}_2\text{PO}_4$ , 0.74 M  $\text{K}_2\text{HPO}_4$ ) supplemented with 50  $\mu\text{g}/\text{ml}$  kanamycine. Further, 50 ml of an overnight culture in induction, and 0.2 mM Isopropyl- $\beta$ -D-thiogalactopyranosid (IPTG) was inoculated with 10% (v/v) preculture. In detail, protein expression was initiated by adding 50 ml of an overnight preculture (grown at 37 °C in LB medium) and 0.2 mM IPTG.<sup>[9]</sup> Then, cultivation in shake flasks was performed for 24 h at 22 °C and 220 rpm before cell pellets were collected by centrifugation (20 min, 3494 g, 4 °C) and stored at -20 °C until further purification.

For cell disruption, cell pellets were first resuspended in 30 ml buffer A (50 mM Tris- $\text{SO}_4$ , 300 mM  $\text{Na}_2\text{SO}_4$ , 25 mM imidazole, pH 7.9), supplemented with 1 mg/ml lysozyme and 1 Pierce Protease Inhibitor Mini Tablet (EDTA-free, Life Technologies, Thermo Fisher Scientific), and then subjected to ultrasound sonification on ice for 7 min (cycle: 10 s pulse, 20 s pause). After sonification, cell free extracts were generated by collecting the supernatant after centrifugation (45 min, 18000 g, 4 °C) and subsequent filtration through a syringe filter (0.45  $\mu\text{m}$  pore diameter).

Cell free extracts were loaded (2 ml/min flow rate) on a 5 ml HisTrap FF column (GE Healthcare, Freiburg, Germany), pre-equilibrated with buffer A using an ÄktaStart FPLC system (GE Healthcare). After loading, the column was washed with 10 column volumes of buffer A to remove other proteins. For the elution of His<sub>6</sub>-tagged target proteins, a gradient over 60 ml to 100% buffer B (50 mM Tris- $\text{SO}_4$ , 300 mM  $\text{Na}_2\text{SO}_4$ , 500 mM imidazole, pH 7.9) was used to collect 1 ml fractions. For desalting, fractions with highest UV absorbance were first pooled and then loaded in portions of 15 ml onto an HiPrep 26/10 desalting columns (GE Healthcare), pre-equilibrated with TE buffer (10 mM Tris- $\text{SO}_4$ , 4 mM EDTA, pH 7.9, 10% (v/v) glycerol). Subsequently, proteins of interest were eluted in TE-buffer and 5 ml fractions. Fractions with highest UV absorbance were concentrated using Vivaspin Turbo 15 centrifugation units (Sartorius, Göttingen, Germany) with 10 kDa molecular weight cut-off. Protein concentrations were calculated by measuring absorbances at 280 nm using a NP80 nanophotometer

(Implen, München, Germany) via Lambert-Beer law with molar extinction coefficients and molecular weights obtained from ProtParam<sup>[42]</sup>. For variants with extra cysteine substitutions, 5 mM  $\beta$ -mercapto ethanol were added to purification buffers and 5mM dithiotreitol to storage buffer.

### ***Activity and enantioselectivity determination***

To determine specific activities of HheG and its variants, conversions of 20 mM cyclohexene oxide (**1**) with 40 mM sodium azide were investigated in 1.5 ml reaction volumes in 50 mM Tris·SO<sub>4</sub>, pH 7.0 at 22°C (900 rpm in Eppendorf ThermoMixer C). After starting reactions by addition of 50  $\mu$ g enzyme, samples were taken after 1, 3, 5, 10, 15, 30, and 60 min and extracted with an equal volume of *tert*-butyl methyl ether (TBME) containing 0.1% (v/v) *n*-dodecane. Organic phases were dried over MgSO<sub>4</sub> and samples were analyzed by achiral GC (Table S7).<sup>[9]</sup>

When measuring the conversion of CLECs and comparison to soluble enzyme, reactions were performed similarly but this time in 1 ml reaction volumes with 100  $\mu$ g biocatalyst. To evaluate enantioselectivities, product enantiomeric excesses were obtained from 4 h samples by chiral GC described elsewhere.<sup>[17]</sup>

To assess activities in different organic co-solvents, reactions contained 25% (v/v) of co-solvents such as ethanol, methanol, 2-propanol, acetonitrile, dimethylsulfoxide, dimethylformamide. Sampling of duplicate reactions was performed after 4 and 24 h and analyzed by achiral GC.

For activities with increasing concentrations of substrate and co-solvent 2-propanol, reactions were performed under standard conditions. A constant azide concentration of 40 mM was used with different concentrations of substrate **1** (5, 10, 20, 50, 100, 150, or 200 mM). Sampling and achiral GC analysis were performed after 4 and 24 h. Reactions were performed in duplicates.

### ***Crystallization of HheG wild type and variants at different scales***

#### ***Crystallization in 2 $\mu$ l scale in 96-well plates***

For initial crystallization screening, sitting-drop crystallization was performed in 2  $\mu$ l scale using 96-well CrystalQuick SW plates (Greiner Bio-one, Kremsmünster, Austria). Droplets were produced by mixing protein solutions of 18, 20, 22, or 24 mg/ml at a ration of 1:1 with crystallization buffer containing 10 mM HEPES (pH 7.0, 7.3, or 7.5) and 2 to 16% (w/v) PEG4000. Reservoirs for sitting-drop application contained 140  $\mu$ l crystallization buffer. Different conditions were analyzed in triplicates and crystallization success was determined after 72 h incubation at 8 °C using microscope SMZ-171-TLED (Moticeurope, Barcelona, Spain).

#### *Crystallization in 20 µl scale in petri dishes*

To determine crystallization parameters, crystallization was scaled up to 20 µl. Now, sitting-drop crystallization was performed in 20 µl droplets containing optimized protein solution mixed with crystallization buffer (1:1) (Table S2) on cover glass plates. For wild-type HheG, a protein concentration of 32 mg/ml was used in contrast to 24 mg/ml for variant HheG D114C. As reservoir, 3 ml crystallization buffer were placed in a separate, smaller petri dish. For 72 h at 8 °C, droplets (on cover glass) and reservoir (in small petri dish) were placed in a standard petri dish that was sealed with parafilm until microscopic documentation.

#### *Crystallization in 200 µl scale in glass vials*

For preparation of CLECs, crystallization conditions were scaled up to 200 µl. Here, precipitation crystallization was performed for 24 h at 8 °C in 2 ml glass vials by mixing 100-150 µl protein solutions (see above) with 50-100 µl crystallization buffer.

To determine the amount of crystallized protein crystals, samples were centrifuged for 3 min at 400 *g* and the amount of crystallized protein was inferred from the remaining protein absorbance at 280 nm in the supernatant. Crystal sizes were measured using ImageJ software<sup>[43]</sup> to calculate crystal volumes using the formula for a regular six-sided prism (Equation S1).

### ***Cross-linking of HheG wild type and variant D114C***

#### *Cross-linking in 20 µl scale in petri dishes*

After 72 h crystallization, mother liquor was removed from crystals via a paper towel and 20 µl cross-linking solution containing 2 mM BMOE in crystallization buffer were added to collected crystals. After cross-linking for 24 h at 8 °C, cross-linking mother liquor was removed via paper towel. Then, CLECs were submerged in 5 µl 50 mM Tris·SO<sub>4</sub> pH 7.0 and subsequently removed via paper towel. To monitor CLEC stability, CLECs were placed in 20 µl 50 mM Tris·SO<sub>4</sub> pH 7.0 and stored for 72 h at 8 °C following microscopic inspection.

#### *Cross-linking in 200 µl scale in glass vials*

For the evaluation of CLECs under experimental conditions, cross-linking was scaled up to 200 µl by removing crystallization mother liquor after 24 h via centrifugation for 3 min at 400 *g*. Then collected crystals of wild-type HheG and variant D114C were submerged in 200 µl cross-linking solution containing either 5 % (v/v) glutaraldehyde or 2 mM BMOE in crystallization buffer for 24 h at 8 °C. Cross-linking mother liquor was removed from CLECs by centrifugation and rinsing with 200 µl 50 mM Tris·SO<sub>4</sub>, pH 7.0. For the evaluation of CLEC thermal stabilities, different CLECs were generated by

varying cross-linking parameters such as the concentration of BMOE (0.5, 1, 2, 5, 10, or 20 mM) and the cross-linking time (3, 6, 18, 24, 48, or 72 h).

### ***Temperature and pH profiles***

To evaluate thermal stabilities, reactions of 1 ml were performed under standard conditions at different temperatures (10, 20, 25, 30, 35, 40, 45, 50, and 60 °C). Samples were taken after 2 h and subsequently analyzed as described above. Maximum conversion was set to 100% relative activity and reactions were performed in duplicate.

Thermal shift assays were performed using a QuantStudio 1 Real-Time-PCR system (Thermo Fisher Scientific) in 50 µl in MicroAmp Optical 96-Well Reaction plates (Thermo Fisher Scientific) containing 5-20 µg protein or CLEC (5 µl), 5 µl 50x concentrated SYPRO orange as fluorescent dye (Thermo Fisher Scientific), and 40 µl TE buffer. Fluorescence (excitation: 580±10 nm, emission: 623±14 nm) was monitored after increasing the temperature in 0.5 °C steps from 10 to 90 °C. The temperature at which the maximum fluorescence change was observed, representing the melting temperature, and which was calculated with the Protein Thermal Shift software (version 1.4, Thermo Fisher Scientific).

For obtaining melting temperatures with different co-solvents, thermal shift assays contained 10% (v/v) of following solvents: ethanol, methanol, 2-propanol, acetonitrile, dimethylsulfoxide, dimethylformamide.

For the determination of melting temperatures at other pH values, 40 µl of TE buffer were replaced by buffers such as 50 mM citrate pH 4-6, 50 mM phosphate pH 6-7, 50 mM Tris-SO<sub>4</sub> pH 7-8.5, or glycine-NaOH pH 8.5-11.

Using the same selection of buffers, activity profiles for different pH values were collected as described above with sampling after 2 h and achiral GC analysis to determine relative activities.

To determine thermal inactivation ( $T_{50}$ ) values of soluble HheG D114C and CLECs, 100 µg of biocatalyst was first incubated for 30 min at different temperatures (10, 20, 30, 32.9, 35.7, 38.6, 41.4, 44.3, 47.1, 50, 60, or 70 °C). Afterwards, residual activity was determined in the conversion of cyclohexene oxide (**1**) with azide using standard reaction conditions (20 mM **1** and 40 mM azide in 50 mM Tris-SO<sub>4</sub>, pH 7.0 at 22 °C and 900 rpm for 2 h). Samples were analyzed by achiral GC analysis (Table S7).

### ***Determination of half-life times***

Half-life times ( $t_{1/2}$ ) of soluble HheG D114C and D114C CLECs at 22 °C were obtained based on the determination of deactivation rate constants ( $k_d$ ). Deactivation rate constants at 30, 32 and 34 °C for soluble enzyme, and 36, 38, 40 °C for CLECs were determined by incubating the enzyme preparations at respective temperatures (T). After 0, 15, 30, 60, 90, 120, 180 and 240 min of incubation, samples were taken for reactions containing 50 µg soluble enzyme or 100 µg CLECs, 20 mM cyclohexene oxide

(1) and 40 mM azide at 22 °C and 900 rpm to determine conversions after 30 min. As the performed reaction of cyclohexene oxide (1) with azide can be described by a pseudo-first order reaction, the natural logarithm of conversion was plotted against time to derive the corresponding deactivation rate constant at a given temperature from the respective slope after linear regression. Plotting  $\ln(k_d/T)$  against  $1/T$  in an Eyring plot (Figure S12) enabled determination of respective deactivation rate constants of both enzyme preparations at 22°C based on the Eyring equation.<sup>[38]</sup> Corresponding deactivation energies ( $E_d$ ) and half-life times ( $t_{1/2}$ ) were calculated using Equations S4 and S5, respectively.<sup>[38,44]</sup>

### **Reuseability**

For the determination of D114C CLEC reuseability, consecutive batch reactions were performed in 1 ml as described in activity section with 100 µg CLECs. After 24 h, samples were taken for achiral and chiral GC analysis (Table S7). Then, remaining reaction mixture was centrifuged for 3 min at 400 g and new reaction medium was added. This procedure was repeated for 21 days with daily sampling in quintuplicates. Similarly, duplicate reactions of 10 mM phenylglycidylether (3), styrene oxide (5), phenylpropylene oxide (7), or limonene oxide (9) with 20 mM azide and 200 µg CLECs were carried out in 50 mM Tris- $\text{SO}_4$  pH 7.0 for 24 h at 22 °C (900 rpm). For five days, daily samples were analyzed by achiral GC and CLECs were reused as for epoxide 1.

### **Crystallization for structure determination**

Crystallization was achieved in 96-well sitting-drop vapor diffusion plates at 277 K using 200 nL of protein solution at a concentration of 23.4 mg/mL mixed with the same volume of precipitant. Plate set-up was performed with a Crystal Gryphon robot (Art Robbins Instruments, Sunnyvale, USA). Crystals were obtained after 24 h. For crosslinking crystals were soaked by adding 0.1 µL of a 0.88 µg/µL BMOE-solution to the crystallization drop followed by 24 h incubation at 277 K. The harvested crystals were cryoprotected in reservoir solution supplemented with 10 % (v/v) (2R,3R)-(-)-2,3-butanediol and flash cooled in liquid nitrogen.

### **Diffraction data collection and structure determination**

Diffraction data were collected with crystals grown in 46 mM HEPES pH 7.34, 5.33 % (w/v) PEG 8000 on beamline P11 (PETRA III synchrotron, DESY, Hamburg, Germany). Data indexing, integration, scaling and reduction was done using the *autoPROC* pipeline.<sup>[45]</sup> Phasing was achieved by molecular replacement with *Phaser*<sup>[46]</sup> using the HheG wildtype structure (PDB ID: 5O30) as a model. An initial model was obtained using *phenix.refine* of the *phenix software suite*<sup>[47]</sup> and completed by manual

adjustments with *Coot*<sup>[48]</sup>. Alternating rounds of manual optimization and *phenix.refine* were used for further refinement. Data collection and refinement statistics are listed in Table S3.

### **Acknowledgement**

We are grateful to the staff of beamline P11 at the PETRAIII synchrotron (DESY campus Hamburg, Germany) for provision of their facilities and assistance in using the beamline. Peer Lukat is especially acknowledged for help with data collection. Additionally, we thank Dr. Felix Kaspar and Dr. Marcus Schallmeyer for helpful advice on the manuscript.

Financial support of M.S. and S.H. by the German Research Foundation (DFG) within the Priority Programme 1934 (DiSPBiotech) and the Research Training Group 2223 (PROCOMPAS), respectively, is gratefully acknowledged.

### **References**

- [1] A. Schallmeyer, M. Schallmeyer, *Appl. Microbiol. Biotechnol.* **2016**, *100*, 7827–7839.
- [2] G. Hasnaoui-Dijoux, M. M. Elenkov, J. H. L. Spelberg, B. Hauer, D. B. Janssen, *ChemBioChem* **2008**, *9*, 1048–1051.
- [3] M. M. Heravi, V. Zadsirjan, B. Farajpour, *RSC Adv.* **2016**, *6*, 30498–30551.
- [4] M. M. Elenkov, H. W. Hoeffken, L. Tang, B. Hauer, D. B. Janssen, *Adv. Synth. Catal.* **2007**, *349*, 2279–2285.
- [5] J. H. Lutje Spelberg, J. E. T. van Hylckama Vlieg, T. Bosma, R. M. Kellogg, D. B. Janssen, *Tetrahedron Asymmetry* **1999**, *10*, 2863–2870.
- [6] M. M. Elenkov, I. Primožič, T. Hrenar, A. Smolko, I. Dokli, B. Salopek-Sondi, L. Tang, *Org. Biomol. Chem.* **2012**, *10*, 5063–5072.
- [7] M. Schallmeyer, J. Koopmeiners, E. Wells, R. Wardenga, A. Schallmeyer, *Appl. Environ. Microbiol.* **2014**, *80*, 7303–7315.
- [8] J. Koopmeiners, B. Halmschlag, M. Schallmeyer, A. Schallmeyer, *Appl. Microbiol. Biotechnol.* **2016**, *100*, 7517–7527.
- [9] J. Koopmeiners, C. Diederich, J. Solarczek, H. Voß, J. Mayer, W. Blankenfeldt, A. Schallmeyer, *ACS Catal.* **2017**, *7*, 6877–6886.
- [10] E. Calderini, J. Wessel, P. Süß, P. Schrepfer, R. Wardenga, A. Schallmeyer, *ChemCatChem* **2019**, *11*, 2099–2106.
- [11] M. An, W. Liu, X. Zhou, R. Ma, H. Wang, B. Cui, W. Han, N. Wan, Y. Chen, *RSC Adv.* **2019**, *9*, 16418–16422.

- [12] R. M. de Jong, K. H. Kalk, L. Tang, D. B. Janssen, B. W. Dijkstra, *J. Bacteriol.* **2006**, *188*, 4051–4056.
- [13] *EMBO J.* **2003**, *22*, 4933–4944.
- [14] F. Watanabe, F. Yu, A. Ohtaki, Y. Yamanaka, K. Noguchi, M. Yohda, M. Odaka, *Proteins* **2015**, *83*, 2230–2239.
- [15] J. Wessel, G. Petrillo, M. Estevez-Gay, S. Bosch, M. Seeger, W. P. Dijkman, J. Iglesias-Fernández, A. Hidalgo, I. Uson, S. Osuna, A. Schallmeyer, *FEBS J.* **2021**, *288*, 4683–4701.
- [16] A. Sharma, J. Agarwal, R. K. Peddinti, *Org. Biomol. Chem.* **2017**, *15*, 1913–1920.
- [17] J. Solarczek, T. Klünemann, F. Brandt, P. Schrepfer, M. Wolter, C. R. Jacob, W. Blankenfeldt, A. Schallmeyer, *Sci. Rep.* **2019**, *9*, 1–10.
- [18] C. Silva, M. Martins, S. Jing, J. Fu, A. Cavaco-Paulo, *Crit. Rev. Biotechnol.* **2018**, *38*, 335–350.
- [19] R. A. Sheldon, S. van Pelt, *Chem. Soc. Rev.* **2013**, *42*, 6223–6235.
- [20] H. Noritomi, K. Koyama, S. Kato, K. Nagahama, *Biotechnol. Tech.* **1998**, *12*, 467–469.
- [21] N. Khalaf, C. P. Govardhan, J. J. Lalonde, R. A. Persichetti, Y.-F. Wang, A. L. Margolin, *J. Am. Chem. Soc.* **1996**, *118*, 5494–5495.
- [22] J. D. Vaghjiani, T. S. Lee, G. J. Lye, M. K. Turner, *Biocatal. Biotransformation* **2000**, *18*, 151–175.
- [23] I. Migneault, C. Dartiguenave, M. J. Bertrand, K. C. Waldron, *BioTechniques* **2004**, *37*, 790–802.
- [24] M. Kubiak, M. Staar, I. Kampen, A. Schallmeyer, C. Schilde, *Crystals* **2021**, *11*, 718.
- [25] B. Smejkal, B. Helk, J.-M. Rondeau, S. Anton, A. Wilke, P. Scheyerer, J. Fries, D. Hekmat, D. Weuster-Botz, *Biotechnol. Bioeng.* **2013**, *110*, 1956–1963.
- [26] B. Jiménez-García, K. Elez, P. I. Koukos, A. M. Bonvin, A. Vangone, *Bioinformatics* **2019**, *35*, 4821–4823.
- [27] J. R. Auclair, K. J. Boggio, G. A. Petsko, D. Ringe, J. N. Agar, *Proc. Natl. Acad. Sci.* **2010**, *107*, 21394–21399.
- [28] M. Kubiak, J. Solarczek, I. Kampen, A. Schallmeyer, A. Kwade, C. Schilde, *Cryst. Growth Des.* **2018**, *18*, 5885–5895.
- [29] Z. S. Derewenda, *Structure* **2004**, *12*, 529–535.
- [30] D. R. Cooper, T. Boczek, K. Grelewska, M. Pinkowska, M. Sikorska, M. Zawadzki, Z. Derewenda, *Acta Crystallogr. D Biol. Crystallogr.* **2007**, *63*, 636–645.
- [31] E. M. Westbrook, P. B. Sigler, *J. Biol. Chem.* **1984**, *259*, 9090–9095.
- [32] J. J. Lalonde, M. Navia, A. L. Margolin, in *Methods Enzymol.*, Academic Press, **1997**, pp. 443–464.
- [33] D. W. Heinz, B. W. Matthews, *Protein Eng. Des. Sel.* **1994**, *7*, 301–307.
- [34] E. Krissinel, K. Henrick, *J. Mol. Biol.* **2007**, *372*, 774–797.
- [35] J. Jegan Roy, T. Emilia Abraham, *Chem. Rev.* **2004**, *104*, 3705–3722.

- [36] P. A. Fitzpatrick, A. C. Steinmetz, D. Ringe, A. M. Klibanov, *Proc. Natl. Acad. Sci.* **1993**, *90*, 8653–8657.
- [37] Z. Wang, G. Zhu, Q. Huang, M. Qian, M. Shao, Y. Jia, Y. Tang, *Biochim. Biophys. Acta BBA - Protein Struct. Mol. Enzymol.* **1998**, *1384*, 335–344.
- [38] Henry. Eyring, A. E. Stearn, *Chem. Rev.* **1939**, *24*, 253–270.
- [39] S. B. Sobolov, M. D. Leonida, A. Bartoszko-Malik, K. I. Voivodov, F. McKinney, J. Kim, A. J. Fry, *J. Org. Chem.* **1996**, *61*, 2125–2128.
- [40] J. J. Roy, T. E. Abraham, *J. Mol. Catal. B Enzym.* **2006**, *38*, 31–36.
- [41] Q. Liao, X. Du, W. Jiang, Y. Tong, Z. Zhao, R. Fang, J. Feng, L. Tang, *J. Biotechnol.* **2018**, 272–273, 48–55.
- [42] E. Gasteiger, C. Hoogland, A. Gattiker, S. Duvaud, M. R. Wilkins, R. D. Appel, A. Bairoch, in *Proteomics Protoc. Handb.* (Ed.: J.M. Walker), Humana Press, Totowa, NJ, **2005**, pp. 571–607.
- [43] WS. RASBAND, <http://imagej.nih.gov/ij/> **2011**.
- [44] K. S. Siddiqui, A. M. Shemsi, M. A. Anwar, M. H. Rashid, M. I. Rajoka, *Enzyme Microb. Technol.* **1999**, *24*, 599–608.
- [45] C. Vonrhein, C. Flensburg, P. Keller, A. Sharff, O. Smart, W. Paciorek, T. Womack, G. Bricogne, *Acta Crystallogr. D Biol. Crystallogr.* **2011**, *67*, 293–302.
- [46] A. J. McCoy, R. W. Grosse-Kunstleve, P. D. Adams, M. D. Winn, L. C. Storoni, R. J. Read, *J. Appl. Crystallogr.* **2007**, *40*, 658–674.
- [47] D. Liebschner, P. V. Afonine, M. L. Baker, G. Bunkoczi, V. B. Chen, T. I. Croll, B. Hintze, L. W. Hung, S. Jain, A. J. McCoy, N. W. Moriarty, R. D. Oeffner, B. K. Poon, M. G. Prisant, R. J. Read, J. S. Richardson, D. C. Richardson, M. D. Sammito, O. V. Sobolev, D. H. Stockwell, T. C. Terwilliger, A. G. Urzhumtsev, L. L. Videau, C. J. Williams, P. D. Adams, *Acta Crystallogr. Sect. Struct. Biol.* **2019**, *75*, 861–877.
- [48] P. Emsley, B. Lohkamp, W. G. Scott, K. Cowtan, *Acta Crystallogr. D Biol. Crystallogr.* **2010**, *66*, 486–501.